MAGNETOHYDRODYNAMICS Vol. 59 (2023), No. 3-4, pp. 347–355
DOI: 10.22364/mhd.59.3-4.7

EIGA-TYPE ELECTRODE MELTING FOR HIGHEST-PURITY CAST PARTS

S. Spitans, H. Franz, B. Sehring, S. Bogner

ALD Vacuum Technologies GmbH, Otto-von-Guericke-Platz 1, 63457 Hanau, Germany

Electrode Induction Melting Inert Gas Atomization (EIGA) is the state-of-the-art process for high-quality spherical powder production. In the EIGA process, the lower end of a vertically hanged pre-alloyed electrode is continuously fed into the region of a $\sim 10^2$ kHz electromagnetic field created by a conical coaxial induction coil located below. Induction melting takes place and a flow in a thin layer is driven at the conical tip of the electrode resulting in a melt stream/dripping down the axis. The application of electrode induction melting for investment casting could be exceptionally beneficial for achieving the highest cleanliness of the cast parts. However, the electrode induction melting for metallic powder production is currently a well-established technique only at relatively small melt rates (such as <2 kg/min). Moreover, the melt cannot be significantly superheated due to the small thickness of the liquid layer at the conical electrode tip and the fact that the material instantly leaks out of the zone of electromagnetic heating as it turns liquid due to the gravity and pinching Lorentz forces. In the present study, we use numerical modelling and experimental validation to demonstrate how the high-melt-rate and high-superheat electrode induction melting can be designed for investment casting applications.

Introduction. The Electrode Induction Melting Inert Gas Atomization (EIGA) process has been developed and patented by ALD Vacuum Technologies [1] as a ceramic-free atomization process that is especially suited for the production of high-purity, reactive and refractory metal powders (Fig. 1*a*). In the EIGA atomization process, the pre-alloyed cylindrical electrode (< 150 mm in diameter and <1 m long) is mounted on the electrode feeding device which continuously lowers the vertically hanged electrode into a conical induction coil. Then, energy is transferred to the electrode tip using a $\sim 10^2$ kHz electromagnetic (EM) field. As a result, a melt film is formed on the electrode surface and a molten metal flows in a stream or forms droplets that fall from the electrode tip into the inert gas nozzle, where a high-velocity gas atomizes the melt [2]. In this way, the generated micro-droplets solidify while traveling downward in the atomization tower and form spherically shaped fine powders which are collected in a vacuum-tight powder container.

Our goal is to investigate whether the advantage of crucible-free electrode induction melting can be combined with investment casting (Fig. 1*b*). In this case, it is crucial to establish a melt flow with a sufficiently high superheat and a melt rate of $60-120$ kg/min, which is typical for a standard Direct Solidification (DS) or Single Crystal (SC) process.

The main advantage of the EIGA-type electrode melting for investment casting is that it is crucible-free. There is no consumable part that has to be regularly replaced and might be a source of ceramic impurities found in castings. Therefore, the guarantee of ultimate casting purity is a clear advantage. Moreover, the EIGA-type electrode melting is very easy to operate. If sufficient power is applied, the system finds the steady-state itself and runs in a self-sustained stable mode. Using the electrode as a feedstock material can save a lot of time – there is no need of charging and discharging the one-shot liner in the back-up crucible. Electrode melting can be stopped anytime and continued later using the next mould. Apart from that, the alloy manufacturer already casts and delivers material in form of cylindrical electrodes, and foundries have to cut the ingot to fit it into the one-shot liner. By avoiding ingot cutting, we can prevent unwanted impurities, approximately 2% of material loss in scrap and additional expenses associated with cutting.

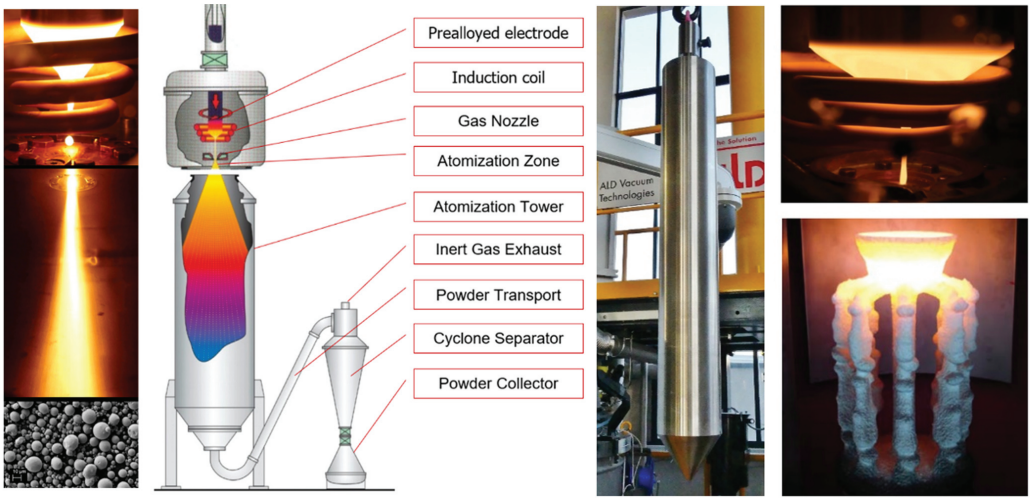

(*a*) (*b*)

Fig. 1. (*a*) The EIGA process and well-established atomization of the 50-mm-diameter Ti64 electrode at a melt rate of 1 kg/min. (*b*) Illustration of the possible EIGA-type 150-mm-diameter Ti64 electrode melting for investment casting application.

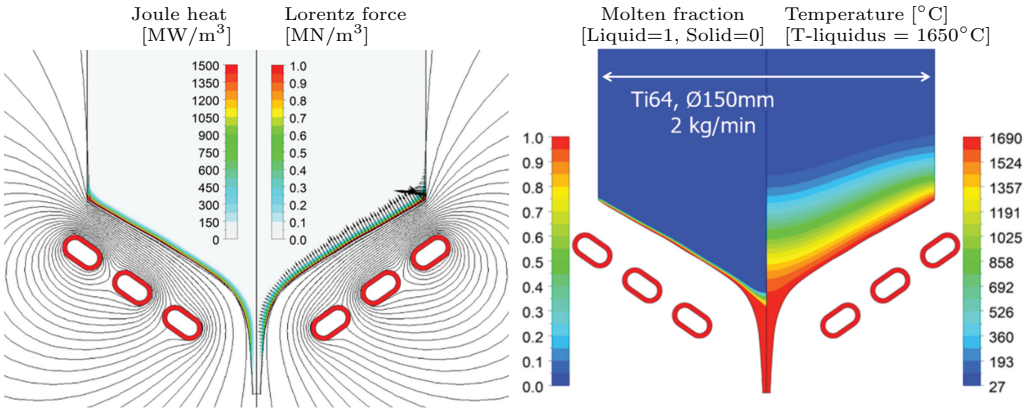

(*a*) (*b*)

Fig. 2. (*a*) Simulation of EIGA-type electrode melting for powder atomization by means of coupling between the EM problem in ANSYS and (*b*) heat transfer + free surface flow problem in FLUENT. The low melt rate (2 kg/min) of the Ti64 electrode (150 mm in diameter) results in a low melt stream superheat of 40°C.

On the other hand, electrode melting at a high melt rate requires high power generators that could be quite expensive. However, due to its high efficiency, the EIGA-type melting still can offer an opportunity for long-term energy saving.

Keeping this in mind, this work focuses on the feasibility study and reveals whether it is possible to achieve a high-melt-rate and a high-superheat melt flow required for investment casting applications. Currently, the well-established melt rates used for powder atomization are below 2 kg/min. Moreover, it is known that during EIGA-type electrode melting, the melt instantly leaks out of the zone of EM heating via a thin layer (short ex-

posure to the EM field). The achieved superheat is low, and this might be a fundamental issue for the casting applications even if higher melting rates are achievable.

Direct melt flow superheat measurement is hardly possible, therefore, our developed and extensively validated model for the liquid metal free surface flow in an AC EM field [3], [4], [5] has been extended to precisely describe the EIGA-type electrode induction melting [6].

To sum up, the computation of EM induced heat transfer, flow and free surface dynamics is ensured by means of coupling between:

• EM field, Lorentz force and Joule heat recalculation upon the frequently updated free surface shape using ANSYS Mechanical APDL (Ansys Parametric Design Language) scripting (Fig. 2*a*).

• Volume of Fluid (VOF) Scale Adaptive Simulation (SAS) of a transient two-phase flow in ANSYS FLUENT for a sufficiently small time-step.

• Free surface shape filtering and reconstruction in ANSYS CFD-Post (Postprocessing software).

The FLUENT model has been supplemented by the heat transfer calculation, including enthalpy-porosity technique for capturing the solidification/melting process and continuous casting approach for modelling the downward movement of the electrode (Fig. 2*b*).

According to our simulation results, the melt stream superheat reaches only 40°C during melting a 150 mm diameter Ti64 electrode at a rate of 2 kg/min. Insufficient superheat was indirectly confirmed by the formation of flakes instead of powder in the powder atomization experiments.

A detailed investigation of the EIGA-type electrode melting using numerical modelling has been of interest for many research groups [7], [8], [9] and is focused on the powder production application (powder production relevant small melt rates, smaller electrode diameters, smaller power levels, etc.). In our EIGA-type electrode melting study, we extended the process parameter range to find out whether this melting technique can be applied for investment casting applications.

1. Results of numerical modelling.

All simulations were performed using a constant alternating current (AC) frequency of $f_{AC} = 100$ kHz. Values of the effective current I_{ef} passing in the oscillation circuit for each simulated configuration are shown in the graphs. An important parameter that is kept constant for further studies in subsections 1.1, 1.2 and 1.3 is the gap between

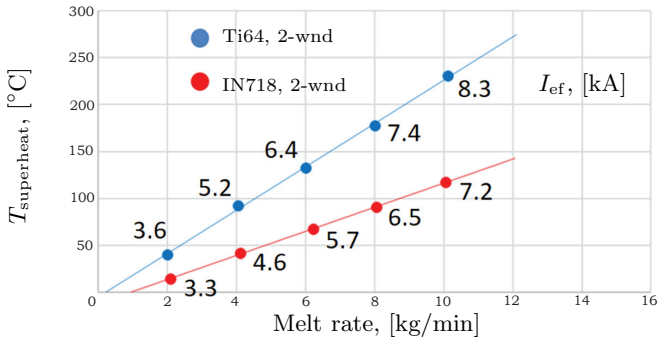

Fig. 3. Steady-state volume-averaged melt stream superheat vs. melt rate for the 150-mm-diameter Ti64 (blue) and IN718 (red) electrodes molten by a two-winding inductor.

the coil and the electrode tip (controlled by an inductance value in the EM problem), because this distance determines the melting efficiency.

1.1. Melt rate. The simulation revealed that the increase of the melt rate leads to a favourable increase of the volume-averaged melt stream superheat (Fig. 3). Note a large superheat of almost 250°C that can be achieved for the Ti64 150-mm diameter electrode at a melt rate of 10 kg/min. A typical example: a $D150\,\text{mm} \times L1\,\text{m}$ ingot of Ti64 has a mass of 80 kg and, when being melted at 10 kg/min, the whole ingot will be molten in 8 minutes.

Let us take a look at the steady temperature profile in the electrode (Fig. 4*a*,*c*). Somewhere far away above the melting front, the electrode is cold, let us say at room temperature. However, closer to the melting interface, the temperature rises and reaches the liquidus temperature at the melting interface. Now, for simplicity of explanation, let us neglect the the latent heat and thermal conductivity dependence on the temperature. If the heat flux passes through the melting front, there must be a temperature gradient that drives it through the molten layer. Or the molten layer temperature at the free surface (for simplicity of explanation, let us neglect heat radiation) should be higher than the liquidus temperature at the melting interface. This is how superheating is still possible in the molten layer (Fig. 4*b*,*d*).

Now, if we double the feeding velocity (equal to the melt rate) and, accordingly, increase the delivered power (the heat flux) to maintain the same melting front location,

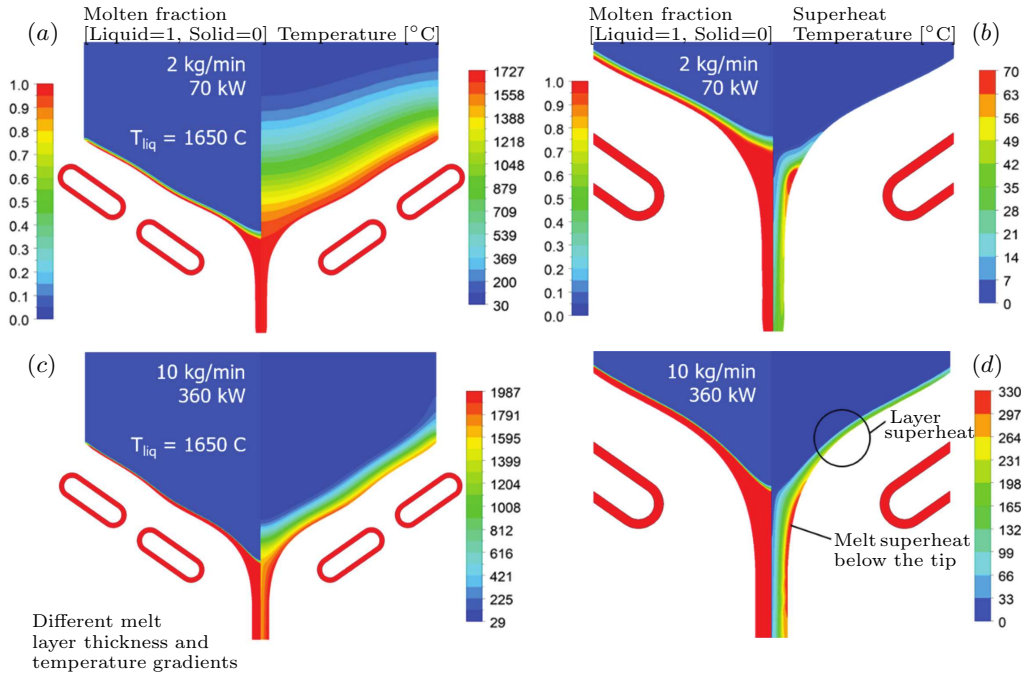

Fig. 4. Contours of the molten fraction/steady temperature (*a*),(*c*) and molten fraction/superheat (*b*),(*d*) in the 150-mm-diameter Ti64 electrode molten at two melt rates: 2 kg/min (*a*),(*b*) and 10 kg/min (*c*),(*d*).

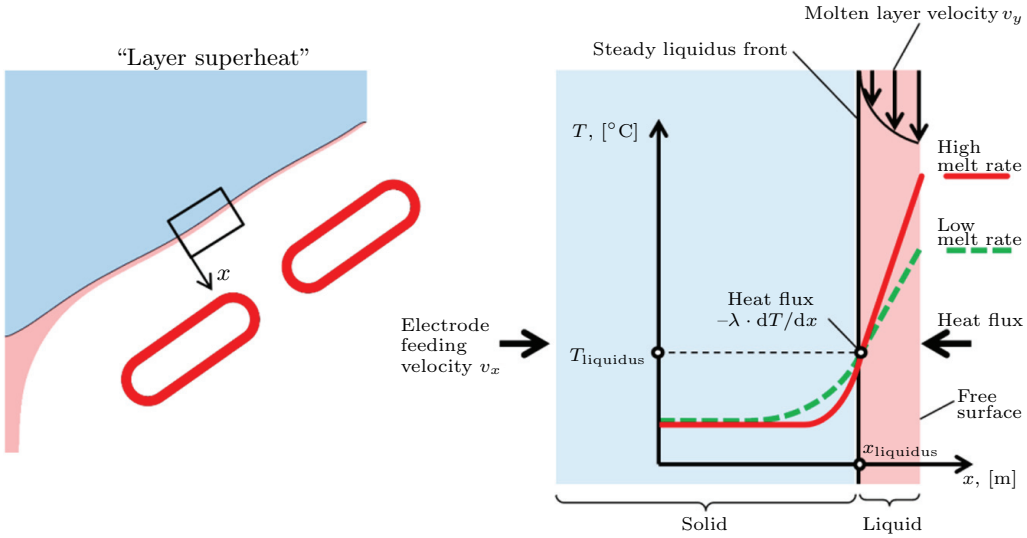

Fig. 5. Mechanism of melt superheat: increased melt rate causes increased melt layer superheat.

the temperature rise in the solid electrode will be steeper and lead to larger superheating in the molten layer (Fig. 5). The larger thickness of the molten layer would also contribute to a larger superheat.

Despite the small superheat caused by the small melt rate in the case of EIGA powder production, the superheat can be significantly increased by increasing the melt rate.

1.2. Alloy. The steepness of linear dependence of the superheat on the melt rate is determined by the alloy thermophysical properties. For example, in case of IN718, less superheat is achieved at the same melt rate, if compare with Ti64 (Fig. 3).

If the density increases (while all other alloy properties are kept the same), the same melt rate requires a less feeding rate, and if the material moves slower, the higher temperature penetrates deeper into the electrode. So, the temperature gradient decreases inside the solid electrode and in the molten layer.

Further superheat decrease is achieved with a higher thermal conductivity, lower liquidus temperature, lower latent heat, lower specific capacity of the solid fraction, etc. or at a larger electrode diameter (equal to slower feeding velocity if the melt rate is maintained constant).

1.3. Inductor design. Actually, it would be more convenient, if we were able to set the melt superheat and the melt rate separately. In this case, the design of the inductor also plays an important role. Here is an example showing that a smaller number of inductor windings allowed us to achieve higher superheat (Fig. 6). All other parameters, including the inductor outer dimensions and AC frequency, were kept the same.

The same melt rate and the same inductor-to-electrode gap require the same magnetic flux density at the surface of the conical tip (or $N \cdot I = \text{const}$, where N is the number of windings, and I is the inductor current). However, an inductor with 4-windings creates a more uniform magnetic flux density at the surface of the conical tip, whereas the current in an inductor with two windings due to the proximity effect passes closer to the

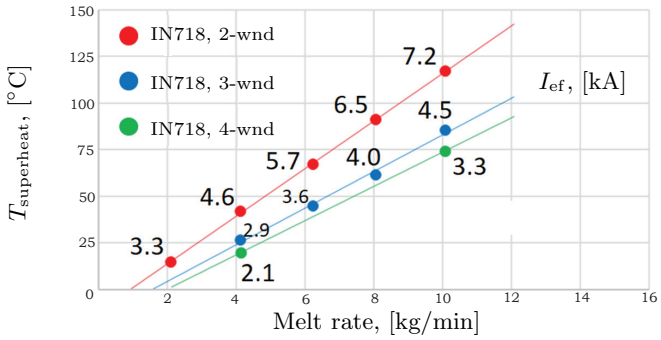

Fig. 6. The 150-mm-diameter IN718 electrode melt stream superheat vs. melt rate is examined for different number of inductor windings: $N = 2$ (red), $N = 3$ (blue) and $N = 4$ (green).

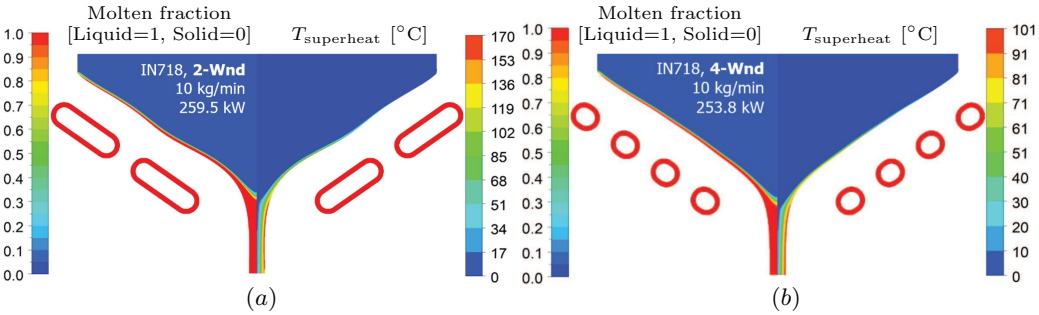

Fig. 7. Contours of the molten fraction and steady superheat distribution in the 150-mm-diameter IN718 electrode molten at 10 kg/min using an inductor (*a*) with two windings and (*b*) with four windings.

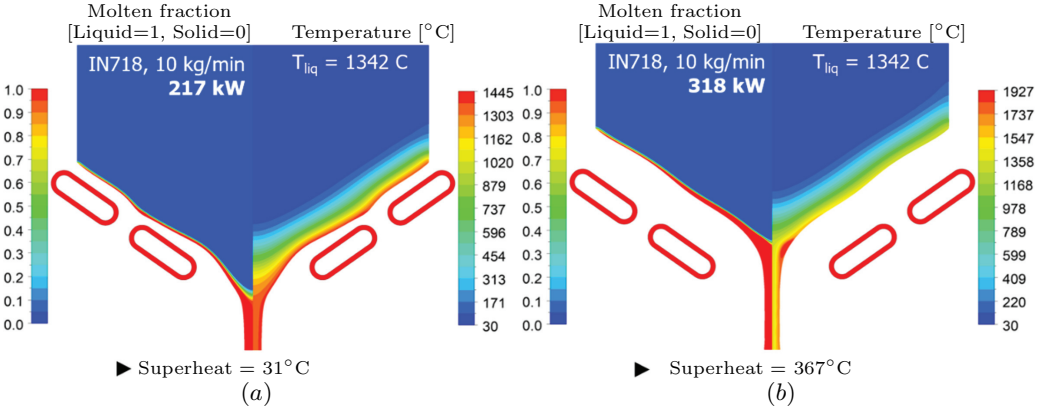

Fig. 8. Contours of the molten fraction and steady temperature distribution in the 150-mm-diameter IN718 electrode molten at 10 kg/min with two different total power levels: (*a*) 217 kW and (*b*) 318 kW.

symmetry axis in each winding and creates a locally stronger magnetic field. Redistribution of the inductor current closer to the axis results in a larger melt stream superheat. Note the shape difference in conical melting fronts caused by different inductor designs (Fig. 7).

1.4. Total power level. Another way to control the superheat independently on the melt rate is to change the level of the total power while keeping other parameters constant. In this case, the gap between the conical inductor tip and the inductor will change as well.

Let us discuss the following experiment: the electrode is being steady-melted at a low total power level. This means that the net power that is induced in the electrode matches the melt rate (or the electrode feeding velocity). What would happen if we instantly increase the total power level? In this case, we would instantly induce much more power in the electrode. However, we should keep in mind that the electrode feeding velocity is maintained constant. So, you would instantly melt faster than you feed the electrode material and the gap between the coil and the electrode would start to enlarge. If the gap enlarges, less net power is induced in the electrode. So the gap will be enlarging unless the net power in the electrode would match again the electrode velocity. This is an amazingly stable and easy to run system that drives itself into a steady regime.

Then, if two electrodes are being melted at the same melt rate and different power levels, smaller superheat will be achieved at lower total power (Fig. 8*a*) and larger superheat at larger total power (Fig. 8*b*). In this case, it has nothing to do with the "layer superheat". In this case, you are superheating the flow below the tip of the electrode. Because of the larger gap between conical electrode tip and inductor and higher power level the melt falls slightly longer through a stronger magnetic field and this results in larger superheat.

So even if the melt rate is fixed, you are able to adjust the superheat by tuning the total power as a separate parameter (Fig. 9) – wide-range contact-free adjustment of the superheat is especially beneficial for large castings.

Steady-state electrode melting is able to ensure a constant desired superheat, whereas preheating of the electrode tip in combination with the increased power at the start of the electrode melting can ensure higher superheat and higher melt rates at the beginning of the mould filling to avoid solidification in the ceramic filter or in the critical zone next to the chill plate.

2. Qualitative validation of simulation results.

Up to now all the simulation results showed that it was possible to achieve higher melt rate and higher superheat during EIGA-type electrode melting. And this brings us closer to fulfilling the requirements of investment casting.

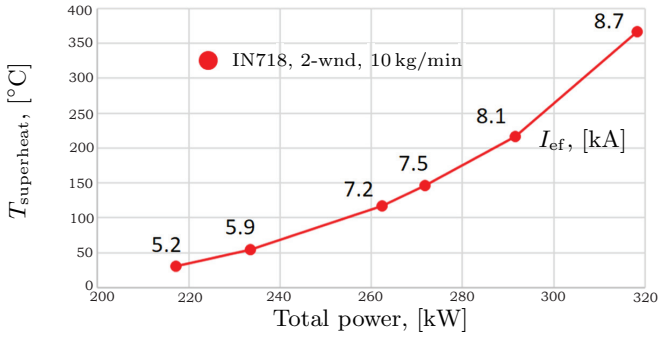

Fig. 9. Steady-state melt stream superheat vs. total power for the 150-mm-diameter IN718 alloy electrode molten at 10 kg/min.

(*a*) (*b*) (*c*) (*d*)

Fig. 10. (*a*) EIGA-type electrode melting and solidification in the copper mould for qualitative validation of simulation results. The solidified Ti64 ingot surface quality obtained at (*b*) 0.5 kg/min and 40 kW , (*c*) 0.5 kg/min and 54 kW, (*d*) 1.0 kg/min and 92 kW.

To validate the simulation results, we decided to carry out an illustative experiment using a real EIGA powder atomization furnace. We disassembled the nozzle and placed a copper mould below the coil and allowed the melt flow to solidify and form the 50-mm diameter ingot (Fig. 10*a*). The surface quality of the ingot would act as a qualitative indicator of the melt superheat.

Note that due to the small melt rates used for powder production, the generator maximum power was only 100 kW.

• Test 1: the reference setting was 0.5 kg/min of Ti64 at a total power of 40 kW. Note the bad surface quality that indicated that the melt solidified before properly filling the mould (Fig. 10*b*).

• Test 2: we maintained the melt rate, but increased the total power up to 54 kW. Note the surface quality improvement that is 100% attributed to the higher superheat (Fig. 10*c*).

• Test 3: we increased both the AC current and the melt rate. The surface quality was the best because of the two effects: (1) higher superheat due to the higher power and higher melt rate, and (2) increased thermal inertia due to the higher melt rate (Fig. 10*d*).

To sum up, the experiment with the real EIGA furnace with the limited generator power has confirmed the results of our simulations. Validation experiments with real castings are planned.

3. Summary and conclusions.

• The melt rates up to 10 kg/min with adjustable superheat between 40 – 400°C have been proven using validated numerical modelling. The total power (and the net power in the electrode) needed to ensure the 10 kg/min melt rate was 360 kW (274 kW) for Ti64 and 260 kW (192 kW) for IN718 using an inductor with two windings. Even higher melt rates are possible but require a proportionally greater power.

• At this stage of the project "EIGA-Type Electrode Melting for Highest-Purity Cast Parts" unsolved issues with the DS/SX investment casting industry have to be discussed: (i) the EIGA-type melt rate (equal to cast rate) is still a rather low compared to the casting rates for the DS/SX process of about 60 kg/min or higher; (ii) adjustment of the casting system of the DS/SX shell mould cluster to the new melting/casting process.

• If the above-mentioned challenges can be overcome, the EIGA-type electrode melting offers attractive advantages over conventional vacuum induction melting with a back-

up crucible and a one-shot liner for the DS/SX process such as: (i) crucible-free (no wear/no consumables), contactless melting; (ii) ultimate casting purity; (iii) easy to operate, reproducible, reliable; (iv) electrode allows for higher productivity and flexibility; (v) higher melting efficiency resulting in a decreased energy consumption for melting.

References

[1] M. Hohmann, N. Ludwig. German Patent DE 4102101 C2, 1991.

[2] X. Li, U. Fritsching. Process modeling pressure-swirl-gas-atomization for metal powder production. *J. Mater. Process. Technol.*, vol. 239 (2017), pp. 1–17.

[3] S. Spitans, A. Jakovics, E. Baake, B. Nacke. Numerical modelling of free surface dynamics of melt in an alternate electromagnetic field. Part I. Implementation and verification of model. *Met. Mat. Trans. B*, vol. 44/3 (2013), pp. 593–605.

[4] S. Spitans, E. Baake, B. Nacke, A. Jakovics. Numerical modelling of free surface dynamics of melt in an alternate electromagnetic field. Part II: conventional electromagnetic levitation. *Met. Mat. Trans. B*, vol. 47/1 (2015), pp. 522–536.

[5] S. Spitans, C. Bauer, H. Franz, B. Sehring, E. Baake. Investment casting with unique levitation melting technology - FastCast. In:*Proc. the Liquid Metal Processing and Casting (LMPC) Conference*, Philadelphia, USA, 2022, pp. 213–222.

[6] S. Spitans, H. Franz, E. Baake. Numerical modeling and optimization of electrode induction melting for inert gas atomization (EIGA). *Met. Mat. Trans. B*, vol. 51/5 (2020), pp. 1918–1927.

[7] V. Bojarevics, A. Roy, K. Pericleous. Numerical model of electrode induction melting for gas atomization. *COMPEL Int. J. Comput. Math. Electr. Electron. Eng.*, vol. 30/5 (2011), pp. 1455–1466.

[8] L. Lu, S. Zhang, J. Xu, H. He, X. Zhao. Numerical study of titanium melting by high frequency inductive heating. *Int. J. Heat. Mass. Transf.*, vol. 108/B (2017), pp. 2021–2028.

[9] H. Li, Y. Shen, P. Liu. Multi-physics coupling simulation of electrode induction melting gas atomization for advanced titanium alloys powder preparation. *Sci. Rep.*, vol. 11 (2021), 23106.

Received 18.12.2023